Nuclear Charge Radii of $^{21-32}$Mg

D. T. Yordanov,[1,2,*] M. L. Bissell,[3] K. Blaum,[1] M. De Rydt,[3] Ch. Geppert,[4] M. Kowalska,[1,2] J. Krämer,[4] K. Kreim,[1] A. Krieger,[4] P. Lievens,[5] T. Neff,[6] R. Neugart,[4] G. Neyens,[3] W. Nörtershäuser,[4,6] R. Sánchez,[4,6] and P. Vingerhoets[3]

[1]*Max-Planck-Institut für Kernphysik, Saupfercheckweg 1, D-69117 Heidelberg, Germany*
[2]*CERN European Organization for Nuclear Research, Physics Department, CH-1211 Geneva 23, Switzerland*
[3]*Instituut voor Kern- en Stralingsfysica, KU Leuven, B-3001 Leuven, Belgium*
[4]*Institut für Kernchemie, Universität Mainz, D-55128 Mainz, Germany*
[5]*Laboratorium voor Vaste-Stoffysica en Magnetisme, KU Leuven, B-3001 Leuven, Belgium*
[6]*GSI Helmholtzzentrum für Schwerionenforschung GmbH, D-64291 Darmstadt, Germany*

(Received 14 October 2011; published 26 January 2012)

Charge radii of all magnesium isotopes in the *sd* shell have been measured, revealing evolution of the nuclear shape throughout two prominent regions of assumed deformation centered on ^{24}Mg and ^{32}Mg. A striking correspondence is found between the nuclear charge radius and the neutron shell structure. The importance of cluster configurations towards $N = 8$ and collectivity near $N = 20$ is discussed in the framework of the fermionic molecular dynamics model. These essential results have been made possible by the first application of laser-induced nuclear orientation for isotope shift measurements.

DOI: 10.1103/PhysRevLett.108.042504 PACS numbers: 21.10.Ft, 27.30.+t, 31.30.Gs, 42.62.Fi

More than three decades set us apart from the first experimental evidence [1–3] prompting Wildenthal and Chung to discuss a ''collapse of the conventional shell-model ordering in the very-neutron-rich isotopes of Na and Mg'' [4]. The associated concept of an ''island of inversion'' has since evolved and many more experimental data have been integrated into the understanding of these nearly magic, yet apparently unpredictable nuclei. Today, as 30 years ago [5], the abnormal data are still attributed to populating the neutron *pf* shell in the presence of *sd* orbitals at a considerable prolate deformation. This idea was repeatedly revisited in recent years to explain new data on nuclear reactions [6–10], spins, and electromagnetic moments [11–16]. The inversion of states in the deformed shell model is directly related to a change in quadrupole deformation [17,18]. In the spherical shell model an adequate description is found, in terms of cross-shell particle-hole excitations ($\hbar\omega$) due to a reduced $N = 20$ shell gap, increased quadrupole collectivity, gain in pairing energy, and the tensor force [19–22]. However, in this approach the deformation does not appear in the sense of a deformed intrinsic state. Therefore, it is difficult to examine to what degree the island of inversion corresponds to an island of deformation. Accommodating the available reaction data and magnetic moments in a common picture is not trivial due to the model dependences in the interpretation of both. As an additional constraint the spectroscopic quadrupole moment is zero for most key isotopes, due to spin zero or one-half, irrespective of the intrinsic deformation. Clearly, there is a need for an observable sensitive to changes in the nuclear shape and common to all isotopes. In this Letter we present an essential step in that direction, a measurement of the rms charge radii. Furthermore, the radii are of critical importance for assessing the role of cluster configurations in the lighter isotopes, where long-range correlations such as in neon [23] are indeed expected. From this perspective our study also explores the applicability of the mean-field description for light nuclei.

Experimentally the charge radii of magnesium present a challenge. The exotic isotopes on both sides of the *sd* shell require an improvement in sensitivity of more than an order of magnitude compared to conventional fluorescence spectroscopy. For other (alkaline-earth or noble-gas) elements state-selective charge exchange [24] and collisional ionization [25] have solved a similar problem, but these rely on specific features in the atomic spectrum. Background rejection by particle-photon coincidence [26] or beam bunching [27] are inapplicable for the cases with considerable beam contamination. Accordingly, we report in this Letter the first application of laser-induced nuclear orientation for high-accuracy isotope shift measurements.

The experiments were carried out with the collinear laser spectroscopy setup [11,16] at ISOLDE-CERN. High-energy protons impinging on a uranium carbide or a silicon carbide target produced neutron-rich or neutron-deficient isotopes, respectively. Magnesium was laser ionized, accelerated to an energy of 50 keV [28] and mass separated. The ion of magnesium (Mg II) was excited in the transition $3s\ ^2S_{1/2} \rightarrow 3p\ ^2P_{1/2}$ (D_1 line at 280.35 nm), which is free of quadrupole interaction and has a well-resolved hyperfine structure. The corresponding ultraviolet light was produced by frequency doubling the output of a stabilized ring dye laser, using Rhodamine 19 as the active medium, pumped at 532 nm. In the conventional manner the atomic transitions were detected by the fluorescence as a function of the Doppler-shifted laser frequency while scanning the ion-beam velocity. The quantity measured was the atomic isotope shift:

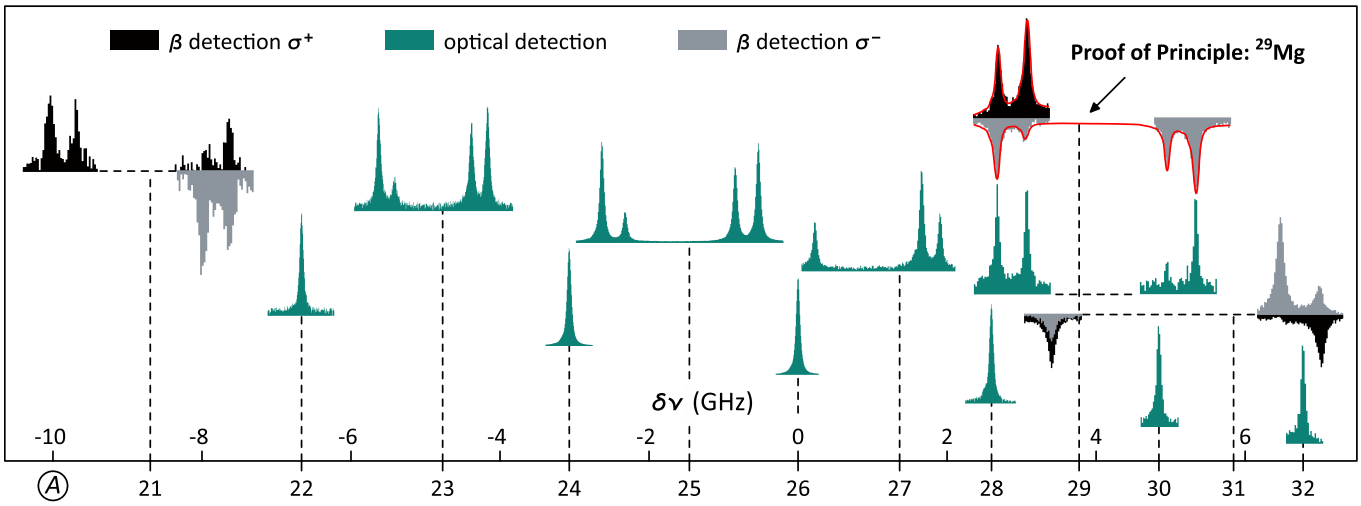

FIG. 1 (color online). Spectral lines of Mg II in the transition $3s\ ^2S_{1/2} \rightarrow 3p\ ^2P_{1/2}$ on a scale relative to the frequency of ^{26}Mg II. The fine structure level of each isotope is represented with a dotted line. All spectra are normalized to a common height. The fitted curves on the β-asymmetry spectra of ^{29}Mg represent the realistic polarization function discussed in the text.

$$\delta\nu^{AA'} = \nu^{A'} - \nu^{A} = K\frac{m_{A'} - m_A}{m_{A'}m_A} + F\delta\langle r^2\rangle^{AA'},$$

with ν^A and $\nu^{A'}$ representing the transition frequencies with respect to the fine structure levels of a reference and a probe isotope, $K = K_{\mathrm{NMS}} + K_{\mathrm{SMS}}$ the sum of the normal and the specific mass shift, m_A and $m_{A'}$ the atomic masses, F the electronic factor, and $\delta\langle r^2\rangle^{AA'} = \langle r^2\rangle^{A'} - \langle r^2\rangle^{A}$ the change in the nuclear mean square charge radius. All measurements used ^{26}Mg [29] as a reference. All isotopes in the range from ^{22}Mg to ^{28}Mg were produced with rates sufficient for fluorescence spectroscopy (above 10^6 ions/s). This method is to a large extent insensitive to the contaminant beams, most notably of sodium and aluminum. In order to enhance the sensitivity to the lower-yield even-even isotopes the photon detection was correlated with the ion beam. In the case of ^{30}Mg ($\approx 5 \times 10^5$ ions/s, $\tau_{1/2} = 335$ ms) the signal was gated on the short release from the target after each proton pulse. True photon-ion coincidence was introduced for the measurements on ^{32}Mg ($\approx 5 \times 10^4$ ions/s), where the ion-beam current also served as a signal normalization against fluctuations of the isotope production. Further use of the coincidence method was limited by the presence of isobaric beam contamination. In addition the sensitivity to nuclei with nonzero spin is generally lower by an order of magnitude. Clearly, the odd isotopes required a different approach.

The application of β-asymmetry detection vastly enhanced the sensitivity and solved the contamination problem by selecting the radioactivity of interest. The atomic angular momenta $\boldsymbol{F} = \boldsymbol{J} + \boldsymbol{I}$ were oriented in the direction of beam propagation by optical pumping with circularly polarized light. A longitudinal magnetic field of 1 mT was used to maintain the polarization axis. The nuclear spin was decoupled from the electron angular momentum by transporting the ion adiabatically into a strong transversal magnetic field of 0.3 T, thus leading to the final nuclear orientation. Excitation in the hyperfine structure transitions was then identified by monitoring the β-decay asymmetry $(N_{0^\circ} - N_{180^\circ})/(N_{0^\circ} + N_{180^\circ})$ after implantation in a MgO crystal.

This orientation method has never been used before as an instrument for investigating isotope shifts. The reason is related to an incomplete control of the orientation process if beams of neutral atoms are used. This was realized in the work on sodium [11] when numerical simulations of the optical pumping process were introduced. In the present work the magnesium ions only interact with the laser light in a well-defined section of constant electrical potential and small longitudinal magnetic field. It was shown [16] that under such conditions the numerical simulations have the potential to quantify the β-asymmetry spectra. For this purpose one needs to solve a system of rate equations $\dot{N} = \hat{M} \cdot N$ for each excitation frequency. Here N is the vector of population densities, $\dot{N} = dN/dt$ and $\hat{M}$ is a $n \times n$ matrix involving the Einstein coefficients, where $n = 2(2I + 1)(J_{\mathrm{lower}} + J_{\mathrm{upper}} + 1)$. Following population transfer in the adiabatic passage to the Paschen-Back regime the orientation is translated from atomic into nuclear. This procedure provides the basis for a realistic polarization function developed to fit the experimental spectra. The equivalence between fluorescence and β-asymmetry detection was investigated on the basis of ^{29}Mg (Fig. 1). This nuclide was accessible by both methods due to its high production rate ($\approx 10^6$ ions/s) and sufficiently short half-life with respect to relaxation times ($\tau_{1/2} = 1.3$ s). The corresponding isotope shifts (Table I) were found consistent within about 2 standard deviations. The small discrepancy may have a statistical origin or could be related to slightly different experimental conditions. The *sd* shell

was completed by measurements with the new method on ^{31}Mg ($\approx 2 \times 10^5$ ions/s) and ^{21}Mg ($\approx 5 \times 10^4$ ions/s). Degrader plates were used in the latter case [30] to shield the detectors from the contaminant beam, whose β decay is much less energetic. By recording the hyperfine structure with left-hand and right-hand circular laser polarization and fitting both simultaneously, one is able to extract information on the magnetic field and the laser power in a self-consistent way. Apart from the moments, radii, and spins the new method is also sensitive to the value and sign of the integral β-decay asymmetry parameter. This quantity can be used, for instance, to aid spin-parity assignments in the daughter nuclei. Such a discussion, however, as well as a detailed description of the numerical approach extend beyond the scope of this Letter and will be published separately.

Typical spectra of all studied isotopes are shown in Fig. 1. Changes in mean square charge radii are extracted from the isotope shifts through a King-plot procedure using the radii [31] of the stable isotopes. The corresponding specific mass shift and the electronic factor of the transition are in excellent agreement with theory [32]. All results are presented in Table I. The systematic errors of the isotope shifts correspond to a 10^{-4} relative uncertainty of the beam energy [28]. These do not influence the extracted radii as they only affect the mass shifts obtained from the King plot [33,34]. This means the accuracy of the radii differences and the absolute radii is essentially determined by the uncertainties of the reference radii. Hence, the corresponding systematic errors are correlated and play no role for the physics discussion.

The total rms charge radii of magnesium spanning the complete *sd* shell are plotted in Fig. 2(a). Clearly, the experimental points lie on three separate slopes signifying three distinct modes of the nuclear size along the chain. This is also evident in Fig. 2(b), which in essence represents the derivative. The physical meaning of the differential plot is an increase of the mean square charge radius by the addition of two neutrons. There is a striking correspondence between the data points and the neutron *sd* orbitals. Beginning with ^{21}Mg the charge distribution is compressed with filling the $d_{5/2}$ orbital up to ^{26}Mg ($N = 14$). A similar effect has also been observed in neon [23,34]. The addition of two neutrons on either $s_{1/2}$ or $d_{3/2}$ in the range $^{28\text{-}30}$Mg results in a steady increase of the radius represented by the middle level in Fig. 2(b). Finally, ^{31}Mg and ^{32}Mg define a third level, which is associated with the island of inversion and in terms of the shell structure would correspond to a cross-shell excitation of two neutrons [12,21]. In ^{27}Mg one of the neutrons added to ^{25}Mg fills the last $d_{5/2}$ hole and the other populates the $s_{1/2}$ subshell, resulting in the intermediate position in Fig. 2(b). Already from a general perspective three important conclusions can be made. First, an island "of inversion" does exist in terms of the rms charge radius and has a well-defined border between

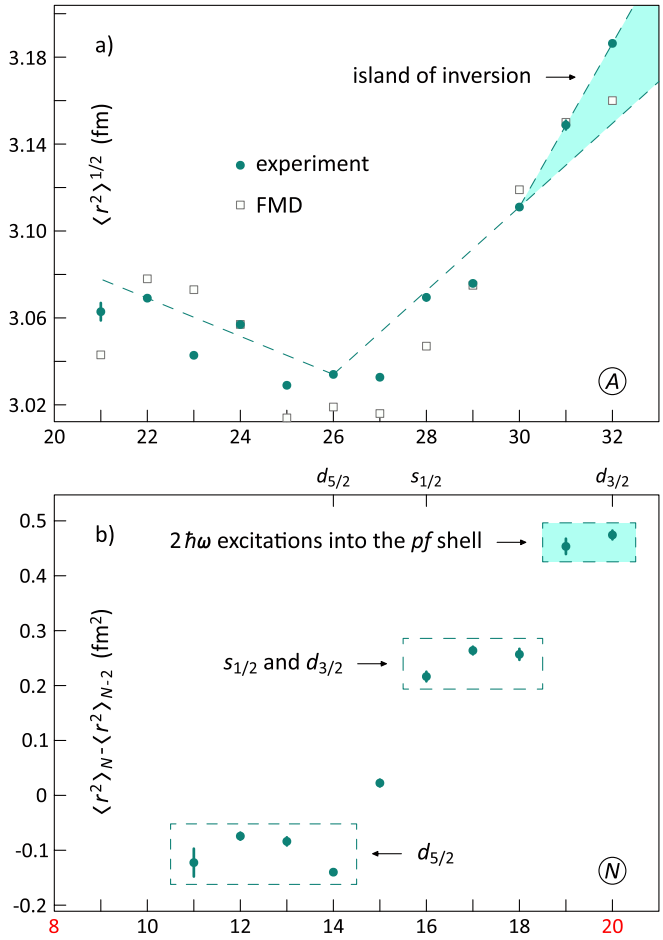

FIG. 2 (color online). Experimental rms charge radii of magnesium (a) compared to theory and differential mean square radii (b). The correlated systematic uncertainties (Table I) are not depicted. Dotted lines and boxes have an illustrative purpose only.

^{30}Mg and ^{31}Mg, as previously anticipated [12,35]. Second, the odd-even staggering is well pronounced except for ^{31}Mg. This indicates a structural change with a prominent effect already in the first isotope of the island. Third, the charge (proton) distribution is strongly correlated with the neutron shell structure.

The role of the quadrupole deformation in the above observations needs to be disentangled from other effects that may contribute. In the mean-field picture the addition of neutrons increases the radius of the mean field for protons, causing the proton distribution to expand. More neutrons also support more binding for protons as the proton-neutron interaction is more attractive than the proton-proton interaction, thus causing the charge distribution to shrink. Alternatively, in the spherical shell model changing trends of the charge radii could be considered as changing contributions from the two major oscillator shells involved, which have different radii and may be associated with different polarizations of the proton distribution. In an attempt to understand these mechanisms we employ the

TABLE I. Nuclear charge radii of $^{21-32}$Mg and isotope shifts of Mg II in the transition $3s\ ^2S_{1/2} \rightarrow 3p\ ^2P_{1/2}$. The statistical and the systematic uncertainties are presented in round and square brackets, respectively.

A	$\delta\nu^{26,A}$ (MHz)	$\delta\langle r^2\rangle^{26,A}$ (fm^2)	$\langle r^2\rangle^{1/2}$ (fm)
21	−8694.3 (31) [345]	0.176 (24) [63]	3.0629 (40) [106]
22	−6663.7 (6) [264]	0.214 (5) [51]	3.0691 (7) [86]
23	−4770.8 (8) [190]	0.053 (6) [34]	3.0428 (10) [61]
24	−3070.6 (7) [122][a,b]	0.140 (5) [25]	3.0570 (7) [48]
25	−1458.5 (6) [58][a]	−0.030 (4) [11]	3.0290 (7) [31]
26	0	0	3.0340 (26)[c]
27	1363.1 (5) [57]	−0.008 (4) [10]	3.0327 (7) [30]
28	2596.5 (11) [118]	0.216 (9) [27]	3.0695 (14) [51]
29	3772.2 (7) [160][d]	0.256 (6) [36]	3.0759 (9) [64]
30	4843.2 (6) [207]	0.473 (5) [56]	3.1110 (8) [94]
31	5845.1 (16) [250]	0.710 (13) [79]	3.1488 (20) [127]
32	6778.4 (8) [310]	0.948 (6) [101]	3.1863 (10) [161]

$F = -127(12)$ MHz/fm^2 $\quad K_{\mathrm{SMS}} = 370(4)$ GHz u

[a]Reference shifts of the n-deficient data set, to be compared with −3073.4(9) [128] and −1460.0(23) [62] of the n-rich data set.
[b]To be compared with −3084.905(93) from in-trap work [29].
[c]Reference rms charge radius of ^{26}Mg [31].
[d]To be compared with 3774.9(9) from β-asymmetry detection.

fermionic molecular dynamics approach (FMD). The many-body basis states are given by intrinsic Slater determinants built from Gaussian wave packets projected on parity and angular momentum [36,37]. Compared with the work on neon [23], we slightly modified the spin-orbit strength of the effective interaction for a better description of the island of inversion. The quadrupole deformation β is used in the present calculation as a generator coordinate. In the island of inversion we find two minima as a function of β corresponding to the normal ($0\hbar\omega$) and the intruder ($2\hbar\omega$) configuration. The matter densities of the two are explicitly shown in Fig. 3 for the case of ^{32}Mg. The full wave function is generated by diagonalizing the Hamiltonian using the β-constrained basis states. Calculated rms charge radii for all measured isotopes are presented in Fig. 2(a). Trends in the deformation of the dominant intrinsic state coincide with the evolution of the radii. Strong deformation and correspondingly large radii, related to γ softness and clustering, are found for $^{22-24}$Mg ($\beta_{^{22}\mathrm{Mg}} = 0.40$). Small charge radii are calculated for the less deformed $^{25-27}$Mg ($\beta_{^{26}\mathrm{Mg}} = 0.22$). With the volume expansion towards ^{30}Mg there is a rapid increase of the radii combined with slightly decreasing deformation ($\beta_{^{30}\mathrm{Mg}} = 0.17$). In the island of inversion we find strong deformation for the intruder configurations ($\beta_{^{32}\mathrm{Mg}} = 0.32$) and further increase of the charge radii. Neutron separation energies are reproduced reasonably well except at the border of the island (^{31,32}Mg) where the sd-pf shell gap is overestimated. As a consequence, the $1/2^+$ ground-state configuration of ^{31}Mg [12] appears in the calculation as an excited state. The magnetic moments of the odd isotopes are found close to the experimental values. Most notably this applies for the $1/2^+$ level of ^{31}Mg, suggesting it has the correct structure and adding confidence to its radius presented in Fig. 2(a). The calculated 2_1^+ energies of the even-even isotopes are also in good agreement with experiment. Description of the experimentally observed odd-even staggering would require either a variation after angular-momentum projection or an explicit treatment of pairing. Mean-field calculations using either Gogny or Skyrme force reproduce roughly the general trends with the minimum at $N = 14$, but are mostly concerned with the even-even cases.

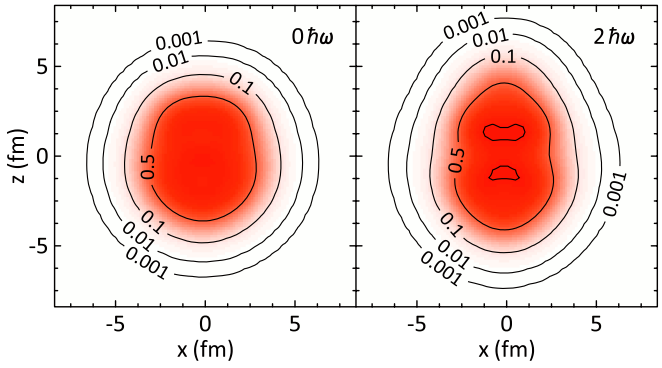

FIG. 3 (color online). Cuts through the matter densities of the intrinsic normal ($0\hbar\omega$) and intruder ($2\hbar\omega$) configurations in ^{32}Mg.

In summary, laser-induced nuclear orientation was combined with fluorescence techniques in order to access all magnesium isotopes in the sd shell. The borderline of the island of inversion was clearly identified between ^{30}Mg and ^{31}Mg. The radial increase towards $N = 8$ is attributed to cluster configurations and γ softness. Both regions were associated with prolate deformation within the fermionic molecular dynamics model. Further theoretical and experimental work is expected to help understand in greater detail the nuclear structure revealed by the rms charge radii.

We are thankful to J.-P. Ebran, T. Rodríguez, and K. Washiyama for providing comparison to mean-field calculations. This work has been supported by the Max-Planck Society, the German Federal Ministry for Education and Research under Contract No. 06MZ9178I, the Helmholtz Association (VH-NG-148), the P6-EURONS (RII3-CT-2004-506065), the BriX IAP Research Program (P6/23), and the FWO-Vlaanderen. A. K. acknowledges support from the Carl Zeiss Stiftung (AZ: 21-0563-2.8/197/1). The authors thank the ISOLDE technical group for their professional assistance.

*Deyan.Yordanov@cern.ch

[1] C. Thibault *et al.*, Phys. Rev. C **12**, 644 (1975).
[2] G. Huber *et al.*, Phys. Rev. C **18**, 2342 (1978).
[3] C. Detraz *et al.*, Phys. Rev. C **19**, 164 (1979).

[4] B. H. Wildenthal and W. Chung, Phys. Rev. C **22**, 2260 (1980).
[5] X. Campi *et al.*, Nucl. Phys. **A251**, 193 (1975).
[6] T. Motobayashi *et al.*, Phys. Lett. B **346**, 9 (1995).
[7] H. Iwasaki *et al.*, Phys. Lett. B **522**, 227 (2001).
[8] Z. Elekes *et al.*, Phys. Rev. C **73**, 044314 (2006).
[9] K. Wimmer *et al.*, Phys. Rev. Lett. **105**, 252501 (2010).
[10] H. T. Fortune, Phys. Rev. C **84**, 024327 (2011).
[11] M. Keim *et al.*, Eur. Phys. J. A **8**, 31 (2000).
[12] G. Neyens *et al.*, Phys. Rev. Lett. **94**, 022501 (2005).
[13] P. Himpe *et al.*, Phys. Lett. B **643**, 257 (2006).
[14] D. Yordanov *et al.*, Phys. Rev. Lett. **99**, 212501 (2007).
[15] P. Himpe *et al.*, Phys. Lett. B **658**, 203 (2008).
[16] M. Kowalska *et al.*, Phys. Rev. C **77**, 034307 (2008).
[17] I. Hamamoto, Phys. Rev. C **76**, 054319 (2007).
[18] D. Yordanov *et al.*, Phys. Rev. Lett. **104**, 129201 (2010).
[19] E. K. Warburton, J. A. Becker, and B. A. Brown, Phys. Rev. C **41**, 1147 (1990).
[20] K. Heyde and J. L. Wood, J. Phys. G **17**, 135 (1991).
[21] A. Poves and J. Retamosa, Phys. Lett. B **184**, 311 (1987).
[22] T. Otsuka *et al.*, Phys. Rev. Lett. **95**, 232502 (2005).
[23] W. Geithner *et al.*, Phys. Rev. Lett. **101**, 252502 (2008).
[24] R. E. Silverans *et al.*, Nucl. Instrum. Methods Phys. Res., Sect. B **26**, 591 (1987).
[25] R. Neugart *et al.*, Nucl. Instrum. Methods Phys. Res., Sect. B **17**, 354 (1986).
[26] D. A. Eastham *et al.*, Opt. Commun. **60**, 293 (1986).
[27] A. Nieminen *et al.*, Phys. Rev. Lett. **88**, 094801 (2002).
[28] A. Krieger *et al.*, Nucl. Instrum. Methods Phys. Res., Sect. A **632**, 23 (2011).
[29] V. Batteiger *et al.*, Phys. Rev. A **80**, 022503 (2009).
[30] J. Krämer *et al.*, Phys. Lett. B **678**, 465 (2009).
[31] G. Fricke and K. Heilig, *Nuclear Charge Radii* (Springer-Verlag, Berlin, Heidelberg, New York, 2004).
[32] B. K. Sahoo, J. Phys. B **43**, 231001 (2010).
[33] A. Klein *et al.*, Nucl. Phys. **A607**, 1 (1996).
[34] K. Marinova *et al.*, Phys. Rev. C **84**, 034313 (2011).
[35] O. Niedermaier *et al.*, Phys. Rev. Lett. **94**, 172501 (2005).
[36] R. Roth *et al.*, Nucl. Phys. **A745**, 3 (2004).
[37] T. Neff and H. Feldmeier, Eur. Phys. J. Special Topics **156**, 69 (2008).